Acta Geodyn. Geomater., Vol. 15, No. 2 (190), 105–115, 2018
DOI: 10.13168/AGG.2018.0012
journal homepage: https://www.irsm.cas.cz/acta

ORIGINAL PAPER

STUDIES ON THE EFFECT OF THE PROPPANT EMBEDMENT PHENOMENON ON THE EFFECTIVE PACKED FRACTURE IN SHALE ROCK

Mateusz MASLOWSKI *, Piotr KASZA and Klaudia WILK

Oil and Gas Institute – National Research Institute, Reservoir Stimulation Department, S. Armii Krajowej 3, 38-400 Krosno, Poland

**Corresponding author's e-mail:* mateusz.maslowski@inig.pl

ARTICLE INFO

Article history:
Received 18 December 2017
Accepted 13 April 2018
Available online 9 May 2018

Keywords:
Embedment
Hydraulic fracturing
Shale
Proppant
Fracture width
Effective packed fracture

ABSTRACT

This paper presents the subject related to the technology of creating fractures into a rock, as well as the subject related to the effect of the proppant embedment phenomenon on the effective packed fracture in a reservoir rock. This phenomenon occurs after the performed hydraulic fracturing treatment of hydrocarbon reservoirs, during closing of the rock mass. A key part of this experiment was to investigate the depth of proppant grains penetration into the fracture wall (shale rock) and size of damage to the fracture wall surface. The embedment phenomena effects on decrease in the width fracture packed with proppant. The tests were performed for shale rock initially soaked with fracturing fluid, lightweight ceramic proppant grains with a grain size of 0.600÷0.300 mm (medium diameter of proppant grains of 0.450 mm), low surface concentration of proppant of 2.44 kg/m^2. Time of exposure of proppant grains to compressive stress of a value 48.3 MPa for 6 hours at 70 ^{o}C. Test results indicate that the developed testing methodology may be used for corrected evaluation of the fracturing fluid as well as proppant in hydraulic fracturing treatment of unconventional reservoirs, especially shale rocks.

INTRODUCTION

For the exploitation of unconventional hydrocarbon reservoirs horizontal wellbores are usually used. Hydraulic fracturing with proppant, which aim to increase the contact surface area between wellbore and reservoirs is performed. The reservoir is fractured due to mechanical effect of fracturing fluid on the rock. The created fractures are then packed with a proppant. This prevents complete closure of the fracture. As a result, the hydrocarbon flow from the reservoir to the wellbore is obtained (Economides and Nolte, 1989; Talib Syed, 2011; Kasza, 2011; Kasza and Wilk, 2012; Masłowski and Czupski, 2014; Masłowski et al., 2016; Masłowski and Biały, 2016), as shown in Figure 1.

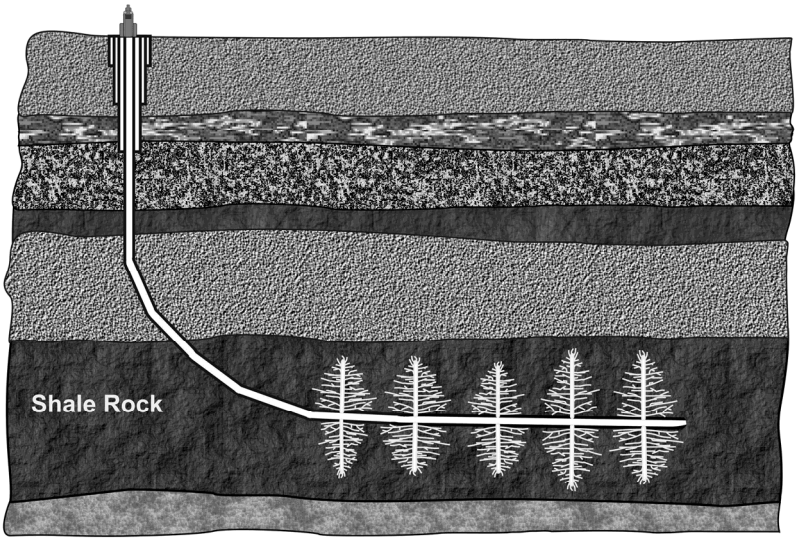

Fig. 1 Schema of the hydraulic fracturing with proppant in unconventional reservoirs.

Cite this article as: Masłowski M, Kasza P, Wilk K: Studies on the effect of the proppant embedment phenomenon on the effective packed fracture in shale rock. Acta Geodyn. Geomater., 15, No. 2 (190), 105–115, 2018. DOI: 10.13168/AGG.2018.0012

In addition to the method of transport and placement of the proppant into a fracture, there is a lot of phenomena, which have a large influence on an effective fracture packing after the hydraulic fracturing treatment. These are: (Economides and Nolte, 1989; Sato and Ichikawa, 1998; Renicke et al., 2006, 2010; Terracina et al., 2010; Alramahi and Sundberg, 2012; Masłowski et al., 2015; Masłowski, 2015; Masłowski et al., 2016)

- poor fracture cleaning from polymers and other additives used in the fracturing fluid from the fracture;
- embedding proppant grains in the fracture faces, so-called embedment;
- crushing, breaking of the proppant grains and compaction of fragments caused by high compression stresses present in the reservoir as well as high temperature;
- reorientation of the proppant grains in the fracture face during its compression;
- proppant grains flowback from the fracture during the return of the fracturing fluid to the wellbore, so-called flowback;
- contamination of sediments during the treatment and exploitation of the hydrocarbon reservoir.

The above listed phenomena are presented in Figure 2.

After the performance of hydraulic fracturing of the reservoir, a decrease of the pressure of pumping the fracturing fluid takes place, thus closing of the fracture (rock mass). This is accompanied by an embedment phenomenon of proppant grains embed into the reservoir rock. It results in increase of the damage to the fracture face, as well as the reduction of the width W_f of the created fracture (Figs. 2 and 3) and decreased of its permeability and conductivity (Sato and Ichikawa, 1998; Legarth et al., 2005; Ghassemi and Suarez-Rivera, 2012; Guo et. al., 2012; Zhang et al., 2014; Masłowski, 2014; Zhang et. al., 2016).

The embedment phenomenon is accompanied by crushing of the deposit rock grains in the area of the fracture faces. This causes the increase of compaction of rock fragments in that area. This results in limitation of the contact surface of the reservoir with the created and packed with proppant fracture. This significantly limits the flow of released hydrocarbons through numerous cracks and microcracks in the reservoir rock to the packed fracture (Reinicke et al., 2006), are presented in Figures 2 and 3.

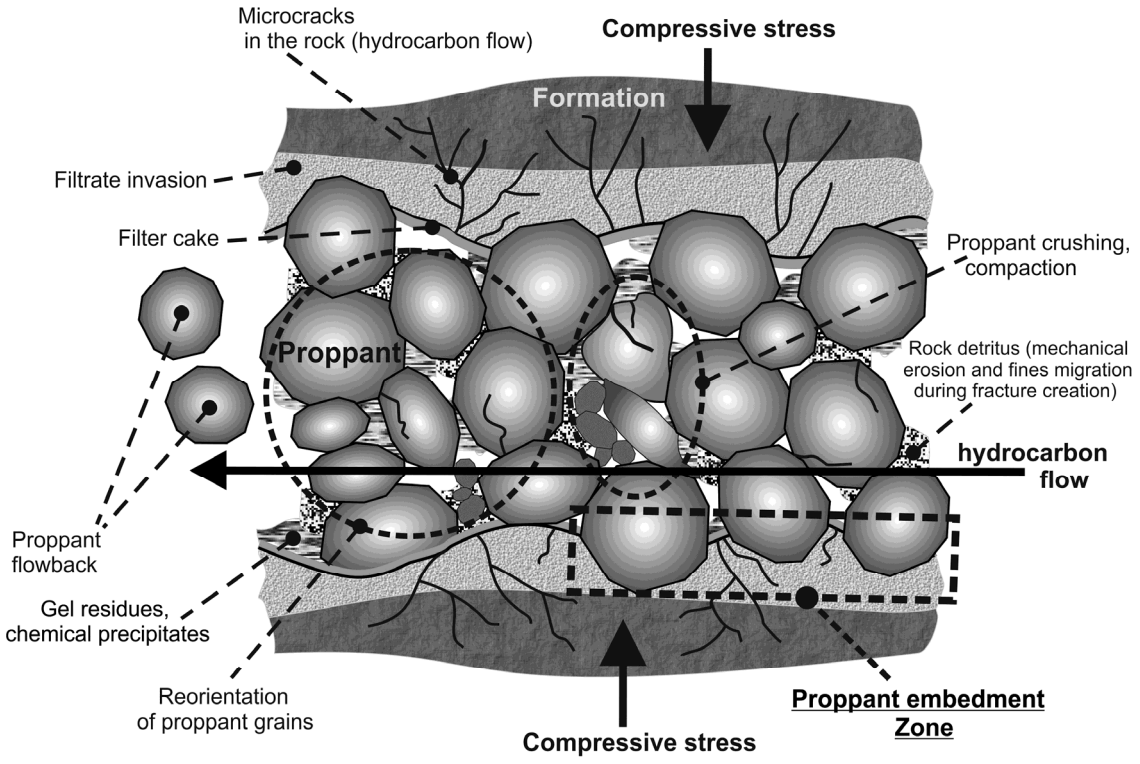

Fig. 2 The phenomena affecting the effective packed fracture, after the hydraulic fracturing of the hydrocarbons reservoáre.

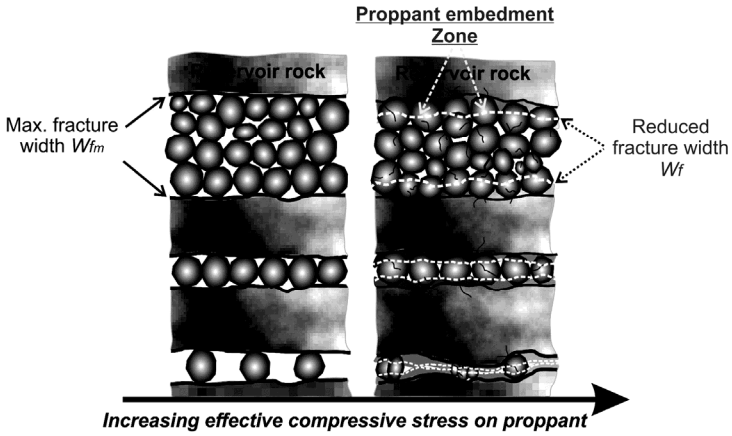

Fig. 3 The effect of embedment phenomenon on the width of the pack fracture, for various proppant surface concentration.

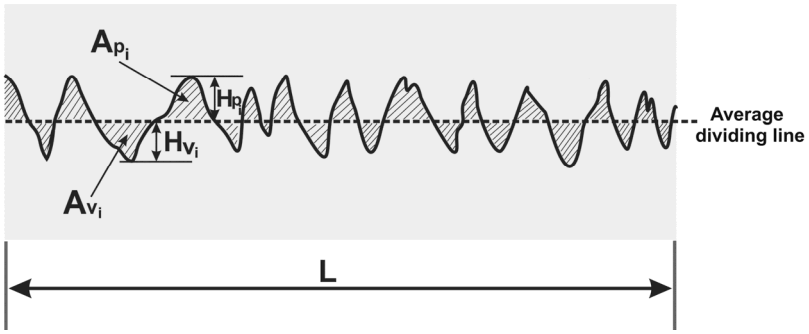

Fig. 4 An example of the surface roughness profile along the measurement section for the selected area, on the surface of the fracture face.

METHODOLOGY OF STUDYING THE EMBEDMENT PHENOMENON

The research methodology developed in INiG-PIG was used (Masłowski et al., 2015; Masłowski, 2015; Masłowski et al., 2016; Masłowski and Biały, 2016). For model purposes, a reference plane (polished surface) was used to determine the phenomenon of embedment. It consists in initial determination of primary roughness of the fracture face. It is determined for several selected areas, and then an average roughness is determined for all of them from the roughness profiles along the selected measurement sections. The method of determination of the surface roughness along the given measurement section is presented in Figure 4 as well as using equations (1) and (2) (Ghassemi and Suarez-Rivera, 2012; Masłowski et al., 2015; Masłowski, 2015; Masłowski et al., 2016; Masłowski and Biały, 2016).

$$\sum_{i=0}^{n} A_{p_i} = \sum_{i=0}^{n} A_{v_i} \tag{1}$$

where: A_p – area of the surface between a peak curve and an average dividing line *(mm²)*; A_v – area of the surface between a valley curve and an average dividing line *(mm²)*

$$R = \frac{\sum_{i=0}^{n} H_{p_i} + \sum_{i=0}^{n} H_{v_i}}{n_p + n_v} \tag{2}$$

where: R – roughness of the profile surface along the measurement section *(mm)*; H_p – peak height *(mm)*; H_v – valley depth *(mm)*; n_p – number of all peaks; n_v – number of all valleys

The average primary roughness R_a for the entire surface of the fracture face is determined as an arithmetic average of roughness of profiles determined for the individually selected areas.

Laboratory simulation of the embedment phenomenon consists in placing a proppant between two cylindrical rock core (Fig. 5) and then exposing it to the set compression stress, in the set temperature, for the set period of time (Fig. 9a), (Masłowski et al., 2015; Masłowski, 2015; Masłowski et al., 2016; Masłowski and Biały, 2016).

The amount of the proppant material needed to pack the fracture and obtain the specified surface concentration is determined according to equation (3), (Masłowski et al., 2015; Masłowski, 2015; Masłowski et al., 2016; Masłowski and Biały, 2016).

$$m_p = A_f \cdot 10^{-1} \cdot C \tag{3}$$

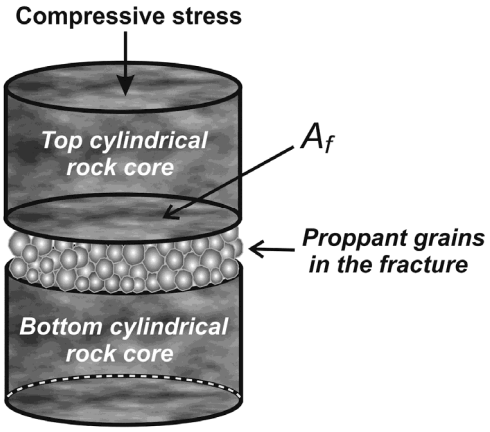

Fig. 5 Schema of placing of the proppant in the fracture during the examination of the embedment of proppant grains in the fracture face.

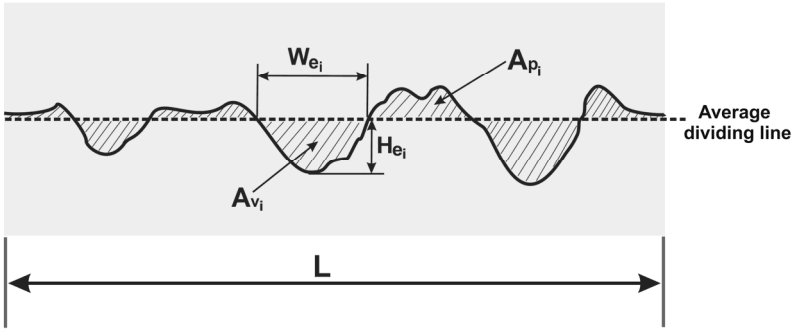

Fig. 6 Sample profile of depth and width of grains embedment (valleys) along the measurement section for the selected area, on the surface of the fracture face.

where: m_p – weight of the proppant *(g)*; C – surface concentration of the proppant *(kg/m^2)*; A_f – surface area of the fracture face subjected to compression stress *(cm^2)*

The analysis of the fracture face after simulation of the embedment phenomenon consists in determination of an average depth of embedment of proppant grains as well as the damage of its surface. The method of determination of the embedment depth as well as the damage of the fracture face along the measurement section are presented in Figure 6 as well as using equations (1) and (4).

$$H_e = \frac{\sum_{i=0}^{n} H_{e_i}}{n_e} \tag{4}$$

where: H_e – average depth of proppant embedment in the fracture face of the profile, along the measurement section *(mm)*; H_{e_i} – valley depth (embedment of a proppant grain in the fracture face) *(mm)*; n_e – amount of all valleys (embedment of proppant grains in the fracture face)

Total average depth He_t of proppant embedment in the fracture faces (rock), expressed in *mm*, is determined according to equation (5).

$$H_{e_t} = H_{e_{T\cdot a}} + H_{e_{B\cdot a}} \tag{5}$$

where: $H_{e_{T\cdot a}}$ – average depth of proppant embedment in the top fracture face, corresponding to arithmetic average of the obtained values for individually specified areas *(mm)*; $H_{e_{B\cdot a}}$ – average depth of proppant embedment in the bottom fracture face, corresponding to arithmetic average of the obtained values for individually specified areas *(mm)*

Percentage damage PDW_e of the fracture surface profile, along the measurement section is determined according to equation (6), expressed in *%*.

$$PDW_e = \frac{\sum_{i=0}^{n} W_{e_i}}{L} \cdot 100\% \tag{6}$$

where: W_{e_i} – valley width, i.e. embedment of a proppant grain in the fracture face *(mm)*; L – length of the measurement section *(mm)*;

Total percentage damage of the fracture surface PDW_{e_t} (embedment of the proppant grains on the surface of the fracture faces) is determined according to equation (7), expressed in *%*.

$$PDW_{e_t} = \frac{PDW_{e_{T\cdot a}} + PDW_{e_{B\cdot a}}}{2} \tag{7}$$

where: $PDW_{e_{T\cdot a}}$ – average percentage damage of the surface of the top fracture face (rock), corresponding to arithmetic average of the obtained values for individually specified areas *(%)*; $PDW_{e_{B\cdot a}}$ – average percentage damage of the surface of the bottom fracture face (rock), corresponding to arithmetic average of the obtained values for individually specified areas *(%)*

The effect of the embedment phenomenon on the effective width of the fracture packed with proppant after exposing to compression stress is determined using equations (8) and (9).

$$W_f = W_{f_m} - H_{e_t} \tag{8}$$

where: W_f – fracture width packed with proppant, taking into account the embedment phenomenon *(mm)*; W_{fm} – maximum fracture width packed with proppant, without the occurrence of the embedment phenomenon *(mm)*

The percentage reduction of the fracture width PRW_f packed with proppant, taking into account the embedment phenomenon is determined according to equation (9), expressed in *%*.

$$PRW_f = \frac{H_{e_t}}{W_{f_m}} \cdot 100 \tag{9}$$

The maximum width W_{fm} of the fracture packed with proppant, without the occurrence of the embedment phenomenon, is determined according to the research procedure previously mentioned in this paper. It only differs in the use of cylindrical steel plugs instead of cylindrical rock cores. They have a steel hardness of more than 43 on the Rockwell C scale (HRC). A maximum width W_{fm} of the fracture packed with proppant was being measured throughout the testing with the use of LVDT device. LVDT readings take into account the amount of deformation of the test unit (i.e. hydraulic press, measuring chamber and steel plugs) under the specified conditions of compressive stress and temperature.

CHARACTERISTICS OF THE RESERVOIR ROCK, FRACTURING FLUID AND PROPPANT MATERIAL USED FOR TRSTINY

Shale rock (Fig. 7.a) was the following mineralogical composition: 47.7 % clay minerals, 24.4 % quartz, 14.2 % carbonates and 13.7 % others minerals. In the Table 1 detailed minerals composition of the shale rock is shown.

A lightweight ceramic proppant 30/50 mesh (Fig. 7b) with a grain size of 0.600÷0.300 mm was used as a proppant material. Water-based fracturing fluid (linear polymer 30#, Fig. 7c) contained in its composition: biocide, gelling agent (guar) 3.6 g/l, clay minerals stabilizer and nanoemulsion.

EXECUTION AND ANALYSIS OF OBTAINED TEST RESULTS OF LABORATORY SIMULATION OF THE EMBEDMENT PHENOMENON

The tests were performed on cylindrical rock cores with a diameter of 2.54 cm, which were cut from the shale rock (Fig. 7a). Subsequently, the top and bottom core faces were polished to obtain a smooth surface (Fig. 8).

Table 1 Quantity analyze of mineral composition based on x-ray diffraction method (XRD). Explanations: percentage by weight: Q – quartz, Pl – plagioclase, K-F – potassium feldspar, C – calcite, D – dolomite, An – ankerite, P – pirite, A – anhydrite, M+l – mica+illite, I/S – mixed-packages illite/smectite, Ch – chlorite, Ot – others minerals, ΣCl – sum of the clay minerals.

Q [%]	*Pl* [%]	*K-F* [%]	*C* [%]	*D* [%]	*An* [%]	*P* [%]	*A* [%]	*M+I* [%]	*I/S* [%]	*Ch* [%]	*Ot* [%]	*Sum* [%]	*ΣCl* [%]
24.4	5.2	2.1	7.2	7.0	2.1	2.8	0.6	36.3	2.9	8.5	9.1	100.1	47.7

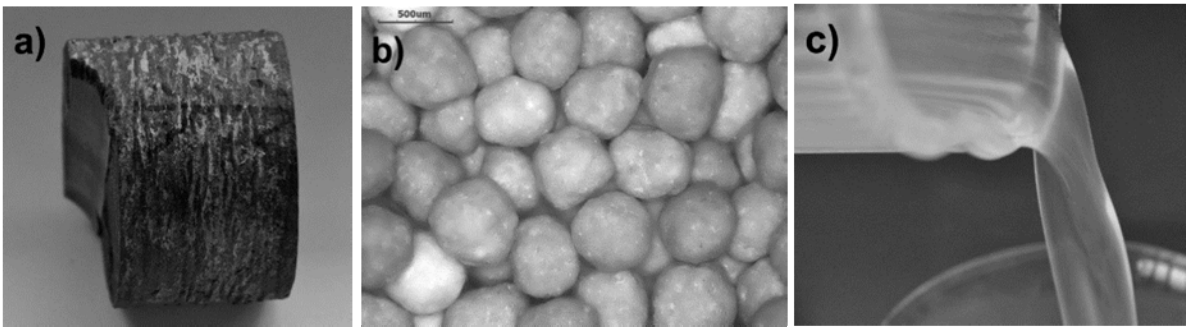

Fig. 7 Materials used for testing: a) Shale rock; b) Proppant; c) Fracturing fluid.

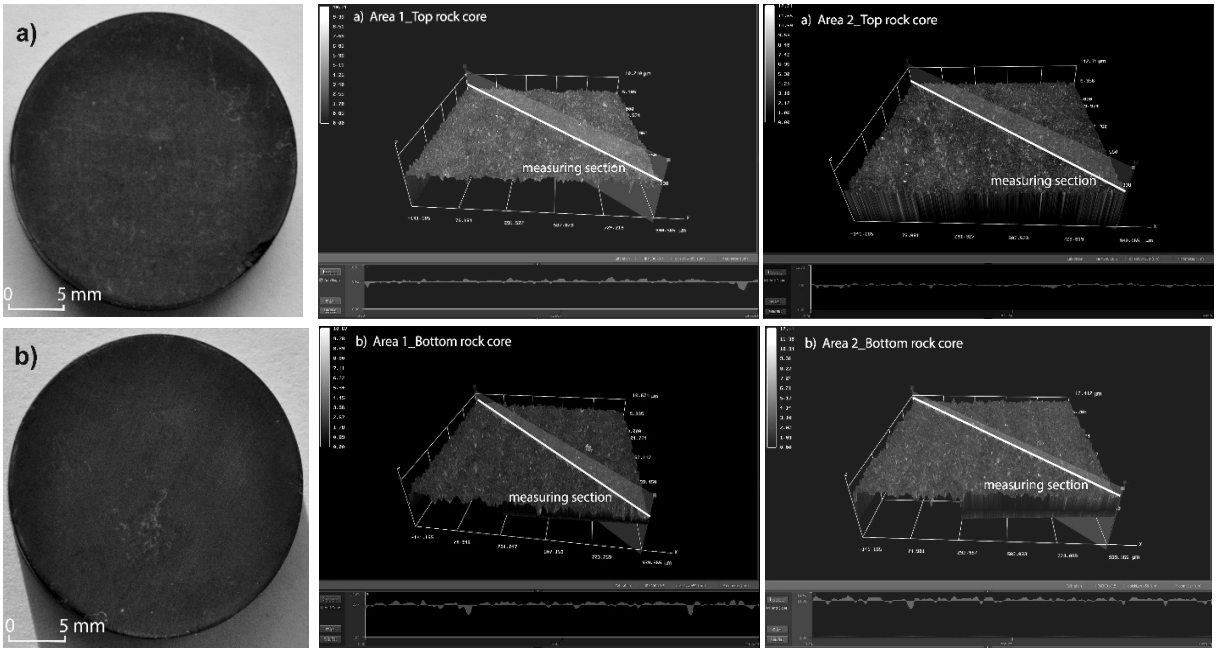

Fig. 8 Determination of the primary roughness for the rock core face (fracture faces): a) top; b) bottom.

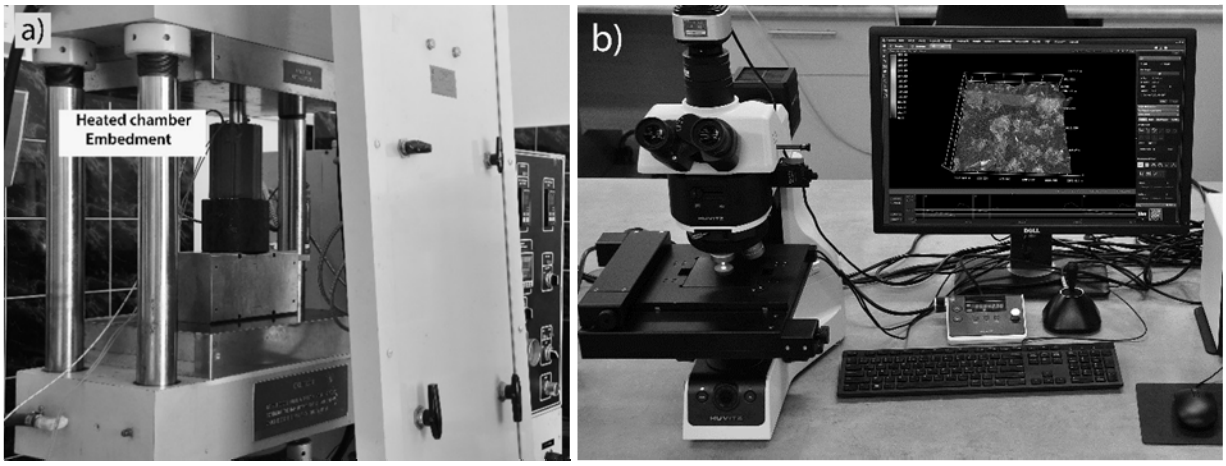

Fig. 9 Test unit: a) Hydraulic press with heating chamber for the simulation of embedment phenomenon; (b) optical microscope with 3D software.

First, the average primary roughness R_a was determined for the entire polished face of the rock. It was determined as an arithmetic average of two selected areas on the face of the tested rock core, from one profile running across the tested area. These tests were performed using an optical microscope, presented in Figure 9b.

The average primary roughness R_a for the entire face of the top rock core (top fracture face) amounted to 0.00042 mm (+/- 0.00005 mm). For the bottom rock core (bottom fracture face) amounted to 0.00065 mm (+/- 0.00017 mm).

Next, laboratory simulation of the phenomenon of proppant embedment in the fracture faces, on the test unit presented in Figures 9a and 9b, was carried out.

The test conditions are presented in Table 2. The rock cores were initially soaked with fracturing fluid at 70 °C and 6.9 MPa for 2 hours.

The temperature of 70 °C and the compressive stress of 48.3 MPa correspond to the average reservoir conditions occurs at the depths of Polish Lower Silurian - Wenlok, shale rock.

The result of test no. 1 is presented in Figures 10, 11, 12 and in Tables 3, 4.

Test no. 2 was performed in order to determine the maximum achievable width of the fracture packed with light ceramic proppant. The conditions of test no. 2 are presented in Table 2. In test no. 2 cylindrical rock cores were replaced with cylindrical steel plugs. After 6 hours of exposition to the defined compressive stress, a W_{fm}, fracture width of 1.514 mm was obtained.

The uncertainty of the estimated width of the fracture packed with proppant was determined based on the accuracy of the LVDT fracture gauge (+/- 0.001 mm). The uncertainty of the estimated total

Table 2 Conditions for the test nos. 1 and 2.

Conditions for test	
Temperature, ^oC	70.0
Surface concentration of proppant, kg/m^2	2.44
Compressive stress, *MPa*	48.3
Exposure to the defined compressive stress, *hours*	6

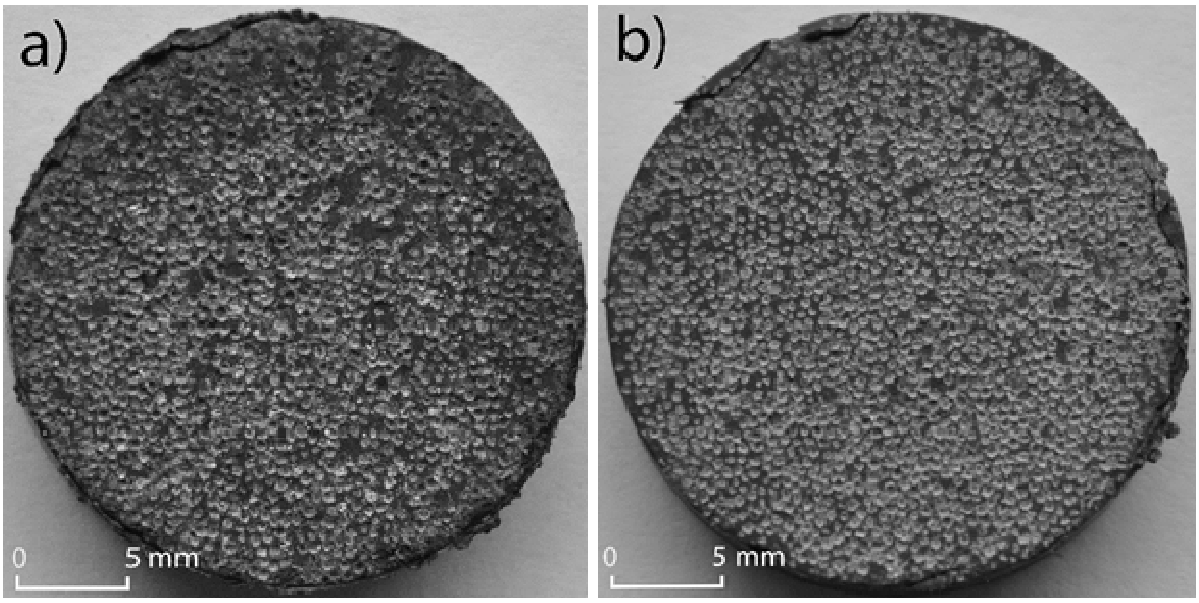

Fig. 10 Surface of the rock core sample: a) top; b) bottom.

Table 3 Total average depth of proppant embedment in the fracture faces – Test 1.

Fracture face	No. of the tested area	Surface area [mm^2]	Average measurement section length [mm]	Total measurement sections length [mm]	He_e [mm]	He_a [mm]	He_t [mm]
Top	1	6.9737	2.7388	10.9551	0.0516	0.0540	
	2	6.9533	2.8153	11.2610	0.0564	+/-0.0034	**0.0890**
Bottom	1	6.8848	2.7255	10.9018	0.0279	0.0350	**+/-0.0134**
	2	7.2606	2.7823	11.1292	0.0420	+/-0.0100	

Table 4 Average percentage damage of the fracture surface – Test 1.

Fracture	No. of the tested area	W_e [mm]	PDW_e [%]	$PDWe_a$ [%]	$PDWe_t$ [%]
Top	**1**	4.0358	36.8	42.2	
	2	5.3787	47.6	+/-7.7	**41.2**
Bottom	**1**	3.9806	36.5	40.2	**+/-1.4**
	2	4.8804	43.9	+/-5.2	

average depth of proppant embedding in the fracture faces is determined based on standard deviation from the average value.

Effective fracture proppant packed parameters are presented in Figure 13.

In addition, an attempt was made to simulate the effect of embedment on effective packed fracture with only one proppant layer. The maximum fracture width, corresponding to an average diameter of the tested proppant grains, amounting to 0.450 mm was used for the calculation. The sizes of proppant grains embedment in the fracture face H_{e_t} and surface damage PDW_{e_t} were equal to the value obtained in test no. 1. The results of this analysis are presented in Figure 14.

CONCLUSIONS

The paper presents the effect of embedment phenomenon on effective packed fracture into the reservoir shale rock with an increased content of clay minerals. In the case of shale rock initially soaked

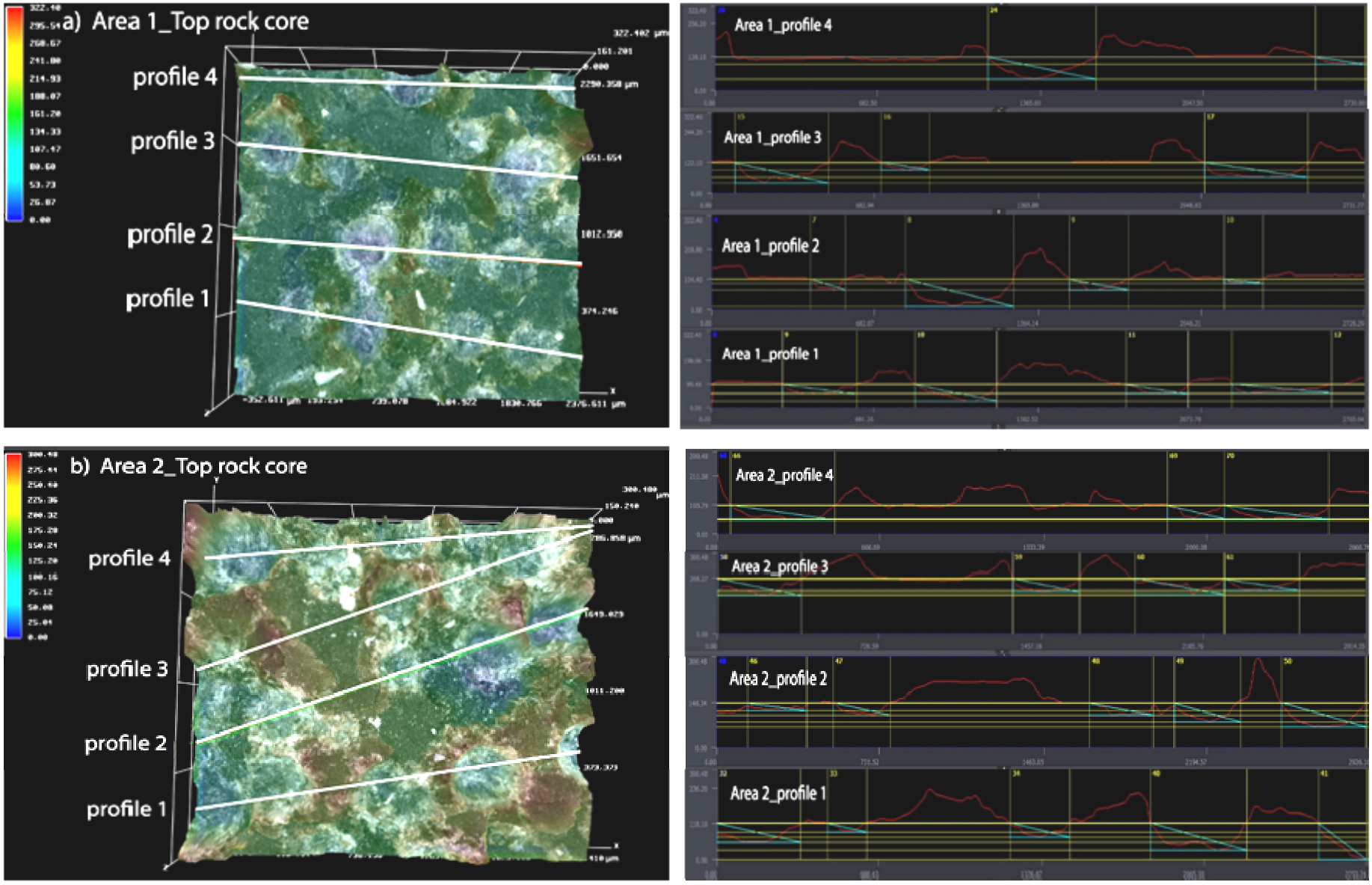

Fig. 11 Average depth $H_{e_{Ta}}$ and average percentage surface damage $PDW_{e_{Ta}}$ for the top rock core (Test 1): a) area 1; b) area 2.

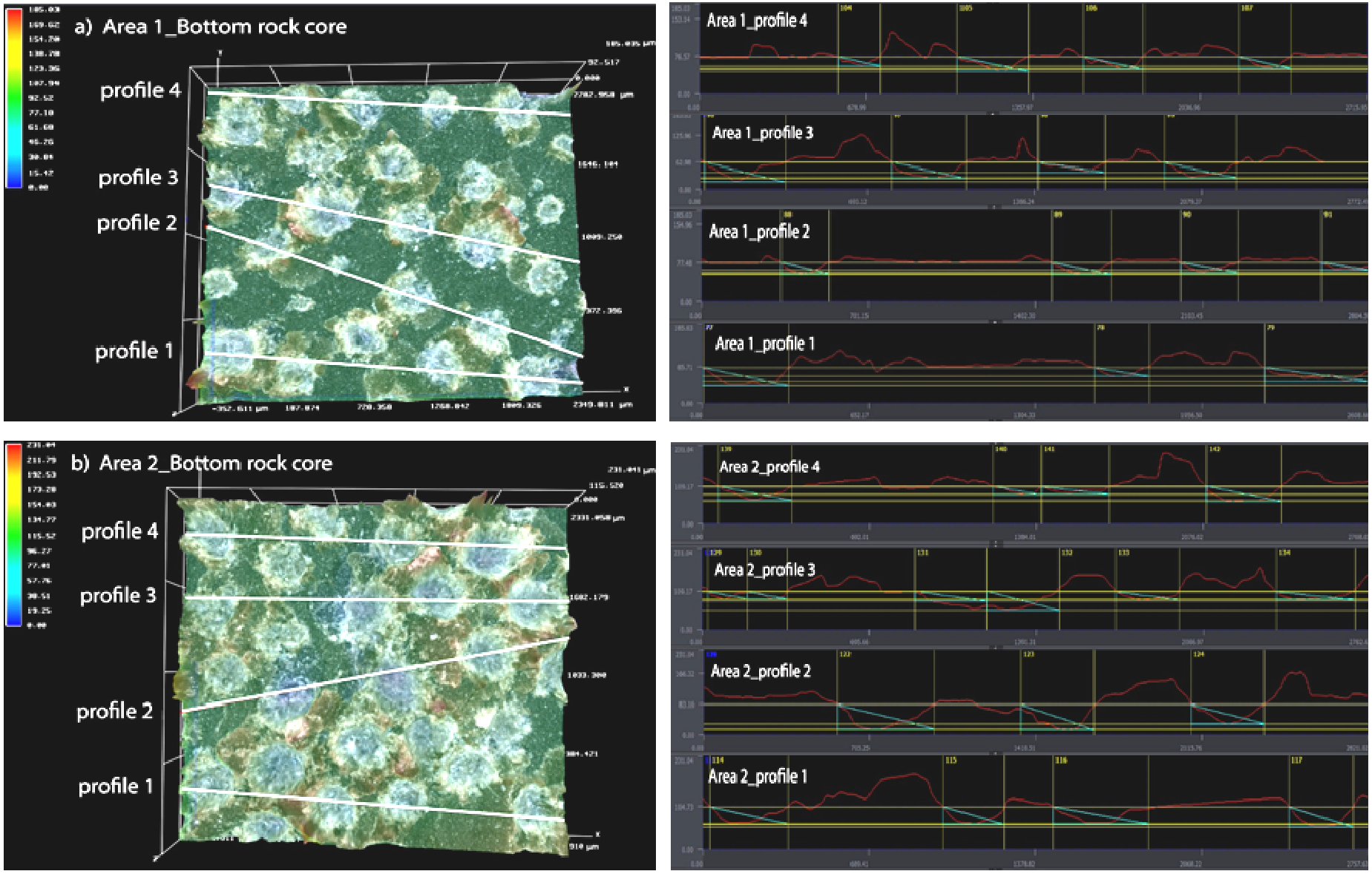

Fig. 12 Average depth $H_{e_{B\text{-}a}}$ and average percentage surface damage $PDW_{e_{B\text{-}a}}$ for the bottom rock core (Test 1): a) area 1; b) area 2.

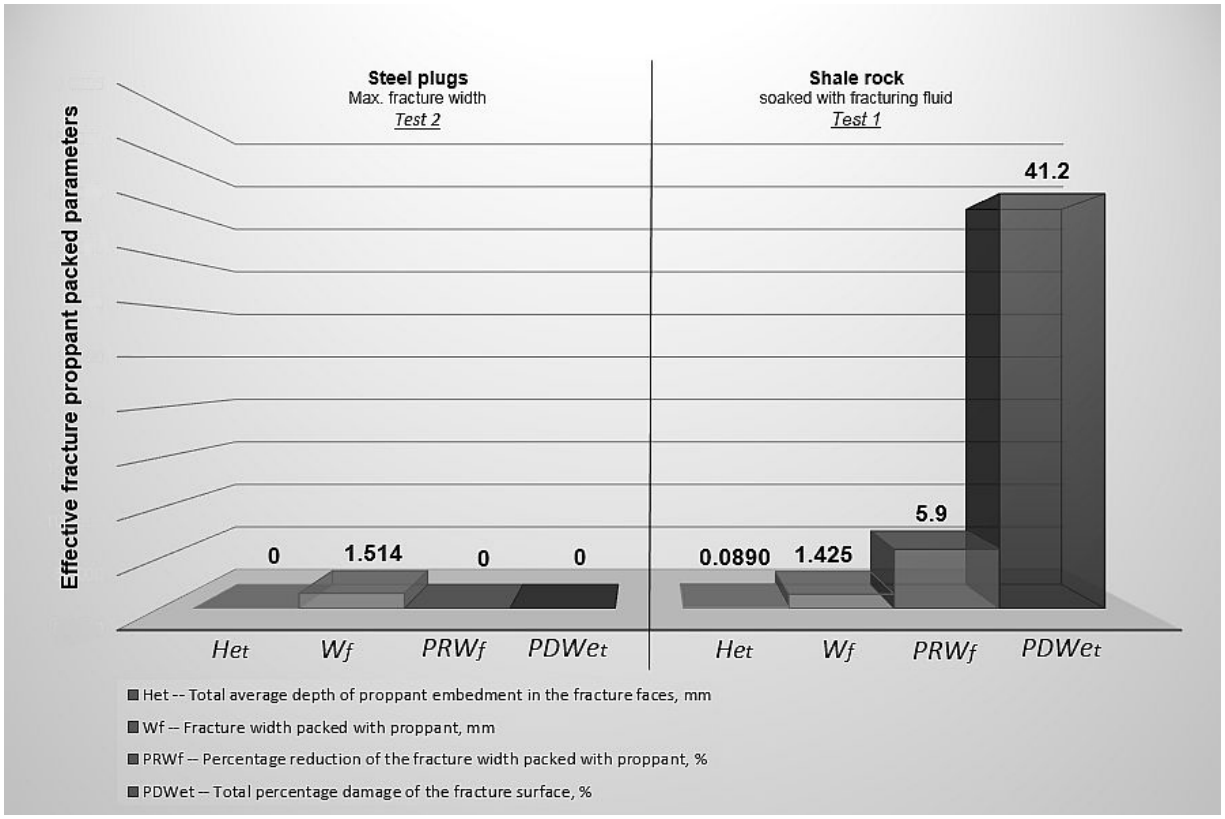

Fig. 13 Effective packed fracture with the proppant for cylindrical steel plugs and shale rock (increased content of clay minerals).

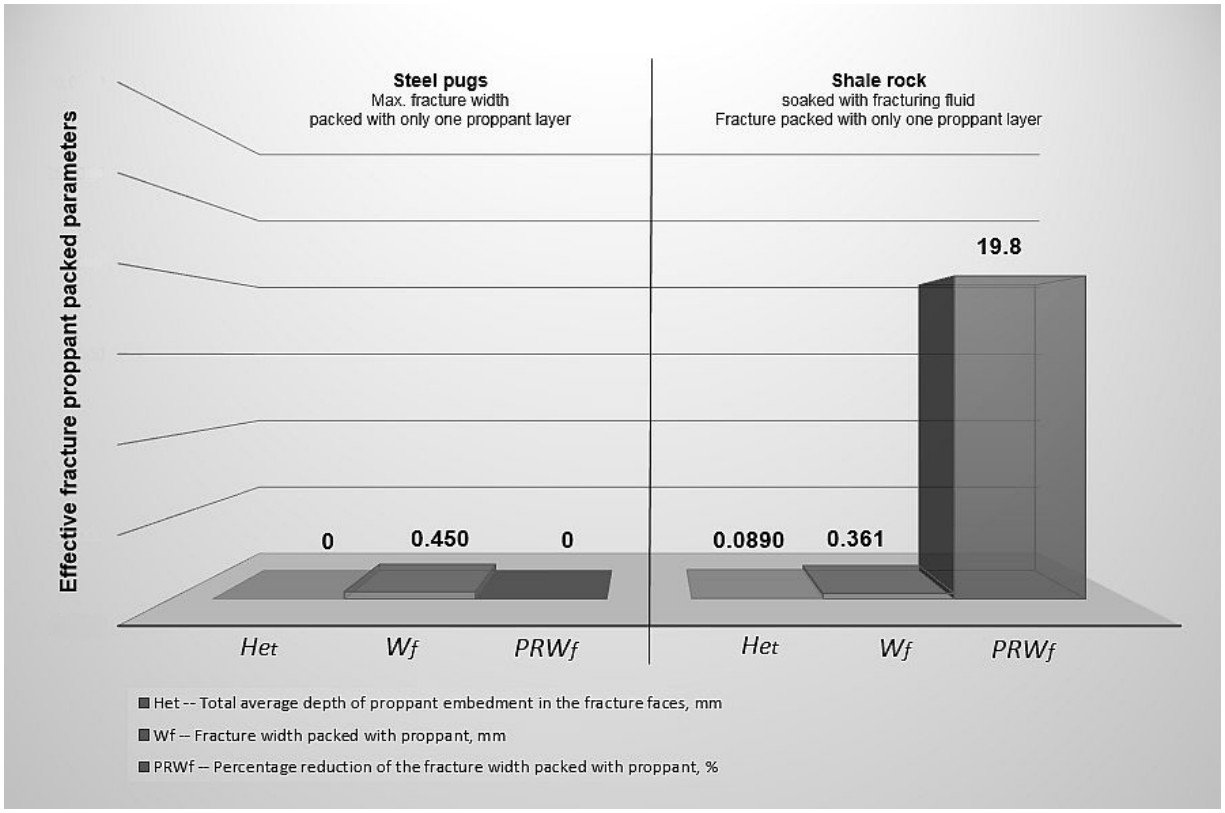

Fig. 14 Effective packed fracture with the proppant for shale rock (increased content of clay minerals) packed with one layer of proppant (grains size 0.600÷0.300 mm).

with the fracturing fluid (linear polymer 30#), a slight decrease in the producer fracture width 0.0890 mm was achieved. The obtained width of the fracture is 1.425 mm, therefore 5.9 % less than the maximum achievable fracture width, which can be 1.514 mm, for the specified test conditions. Concerning the assessment of the fracture surface damage 41.2 % is achieved by the proppant grains. For the additionally simulated maximum fracture width 0.450 mm, corresponding to only one layer of the tested proppant, the decrease in the maximum fracture width by 19.8 % is obtained. In this case, the depth of proppant embedment of 0.0890 mm was used for the calculation. The final width of such packed fracture is 0.361 mm.

The size of the fracture width determines the flow of hydrocarbons from the reservoir to the wellbore. The tested rock has good properties of packed fracture and to ensure the flow of hydrocarbons from the reservoir to the wellbore.

Test results indicate that the developed method of measurement may be one of the preliminary assessment of the proper selection when choosing fracturing fluid and the proppant type for hydraulic fracturing of unconventional reservoirs, especially shale rocks.

ACKNOWLEDGEMENTS

This paper is based on the results from statutory work. Archive no. DK-4100-56/17.

REFERENCES

Alramahi, B. and Sundberg, M.I.: 2012, Proppant embedment and conductivity of hydraulic fractures in Shales. ARMA, 12-291, 1–6.

Economides, M.J. and Nolte, K.G.: 1989, Reservoir Stimulation. Second edition. Houston.

Ghassemi, A. and Suarez-Rivera, R.: 2012, Sustaining fracture area and conductivity of gas shale reservoirs for enhancing long-term production and recovery. Appendix 5 – Proppant embedment standard testing procedure. Research Partnership to Secure Energy for America. Final report of Project no. 08122-48. 15.V.2012.

Guo, J. and Liu, Y.: 2012, Modeling of proppant embedment: Elastic deformation and creep deformation. Paper Society of Petroleum Engineers presented at the SPE International Production and Operations Conference and Exhibition, Doha, Qatar, 14-16 May 2012. SPE 157449-MS. DOI: 10.2118/157449-MS

Kasza, P.: 2011, Production stimulation treatments in the unconventional reservoirs. Nafta-Gaz, 10, 697–701, (in Polish).

Kasza, P. and Wilk, K.: 2012, Completion of shale gas formations by hydraulic fracturing. Przemysł Chemiczny, 4, 608–612, (in Polish).

Legarth, B., Huenges, E. and Zimmermann, G.: 2005, Hydraulic fracturing in a sedimentary geothermal reservoir: Results and implications. Int. J. Rock Mech. Min. Sci., 42, 7-8, 1028–1041. DOI: 10.1016/j.ijrmms-2005.05.014

Masłowski, M.: 2014, Proppant material for hydraulic fracturing in unconventional reservoirs. Nafta-Gaz, 2, 75–86, (in Polish with English summary).

Masłowski, M.: 2015, Studies of the embedment phenomenon after the hydraulic fracturing treatment of unconventional reservoirs. Nafta-Gaz, 7, 461–471, (in Polish with English summary).

Masłowski, M. and Biały, E.: 2016, Studies of the embedment phenomenon in stimulation treatments. Nafta-Gaz, 12, 1101-1106, (in Polish with English summary). DOI: 10.18668/NG.2016.12.13

Masłowski, M. and Czupski, M.: 2014, Basic properties of proppants used in hydraulic fracturing treatments of hydrocarbon deposits. Przegląd Górniczy, 12, 44–50, (in Polish with English summary).

Masłowski, M., Kasza, P. and Czupski, M.: 2016, Studies of the susceptibility of the tight gas rock to the phenomenon of embedment, limiting the effectiveness of hydraulic fracturing. Nafta-Gaz, 10, 822–832, (in Polish with English summary). DOI: 10.18668/NG.2016.10.07

Masłowski, M., Kasza, P., Czupski, M. and Wilk, K.: 2015, A method of determining the reduction of the pack fracture width. Zgłoszenie patentowe nr P.412971, Urząd Patentowy RP, (in Polish).

Reinicke, A., Legarth, B., Zimmermann, G., Huenges E. and Dresenn, G.: 2006, Hydraulic fracturing and formation damage in a sedimentary geothermal reservoir. ENGINE–Enhanced Geothermal Innovative Network for Europe Workshop 3, Stimulation of reservoir and microseismicity, Kartause Ittingen, Zürich, 29, VI – 1.VII, Switzerland.

Reinicke, A. and Rybacki, E., Stanchits, S., Huenges, E. and Dresen, G.: 2010, Hydraulic fracturing stimulation techniques and formation damage mechanisms – Implications from laboratory testing of tight sandstone – proppant systems. Chemie der Erde - Geochemistry, 70, 107–117. DOI: 10.1016/j.chemer.2010.05.016

Sato, K. and Ichikawa, M.: 1998, Post-Frac analysis indicating multiple fractures created in a volcanic formation. Paper Society of Petroleum Engineers presented at the SPE India Oil and Gas Conference and Exhibition, 17-19 February 1998, New Delhi, India. SPE 39513-MS. DOI: 10.2118/39513-MS

Talib Syed, P.E., TSA: 2011, Mechanical integrity Pre and Post well integrity methods for hydraulically fractured/stimulated wells. EPA Hydraulic Fracturing Workshop, Arlington, VA 22202, 10-11.III.2011.

Terracina, J.M., Turner, J.M., Collins, D.H. and Spillars, S.E.: 2010, Proppant selection and its effect on the results of fracturing treatments performed in shale formations. Paper Society of Petroleum Engineers presented at the Annual Technical Conference and Exhibition, 19-22 September, Florence, Italy. SPE 135502. DOI: 10.2118/135502-MS

Zhang, J., Ouyang, L., Hill, A.D. and Zhu, D.: 2014, Experimental and numerical studies of reduced fracture conductivity due to proppant embedment in shale reservoirs. Paper Society of Petroleum Engineers presented at the PE Annual Technical Conference and Exhibition, 27-29 October 2014, Amsterdam, The Netherlands. SPE 170775-MS, 1–15. DOI: 10.2118/170775-MS

Zhang, F., Zhu, H., Zhou, H., Guo, J. and Bo, H.: 2017, Discrete-element-method/computational-fluid-dynamics coupling simulation of proppant embedment and fracture conductivity after hydraulic fracturing. SPE Journal, 22, 632–644. SPE 185172-PA. DOI: 10.2118/185172-PA